Johannes Deiglmayr

HIGHLY EXCITED MOLECULES – THE UNUSUAL PROPERTIES OF MICROMETER-SIZED DIMERS

When we think about a molecule, we mostly consider bonds between elements in their electronic ground state. Can atoms in highly-excited electronic states also form "stable" chemical bonds? How can we calculate the electronic structure of such molecules accurately and efficiently? And how can we study them experimentally? These are questions that we are trying to answer in our research. The basic building blocks of the molecules we study are atoms with a valence electron in a highly-excited orbital, so called "Rydberg atoms". The semiclassical orbit of the Rydberg electron has a radius of $n^2 a_0$, where n is the principal quantum number of the excited state and a_0 is the Bohr radius. Already for $n = 30$, the diameter of a Rydberg atom approaches 100 nm. The resulting strong delocalization of the electronic wavefunction increases also the radiative lifetime, which scales as n^3 and exceeds 30 µs at $n = 30$.

In principle, molecules containing Rydberg atoms could be stable on the same timescale as the Rydberg atom if the only decay mechanism would be radiative decay of the electronic excitation. However, experience tells us that highly-excited molecules typically dissociate or autoionize within pico- to femtoseconds. In the following we will discuss two types of molecules where this is not the case. For the first type of molecules, the binding results purely from long-range van der Waals forces. We demonstrate experimentally that such interactions between two atoms in a Rydberg state, with an internal excitation energy of a few electron volts each, lead to vibrationally stable dimers with binding energies in the micro-eV range, as predicted by theory [1, 2]. For the second type of molecules, the binding results from the scattering of a Rydberg-electron off neutral particles within its orbit. This interaction provides an even more exotic binding mechanism for long-range Rydberg molecules, which is neither ionic, nor of covalent or van der Waals type [3]. This novel binding mechanism, low-energy electron-neutral scattering, plays an important role in the kinetics of cold plasmas and interstellar clouds. We will demonstrate how an accurate modelling of long-range Rydberg molecules can yield reliable experimental values for the relevant scattering parameters.

Dr. Johannes Deiglmayr
Laboratory of Physical Chemistry, ETH Zurich, Switzerland
Vladimir-Prelog-Weg 1-5/10, 8093 Zurich
E-Mail: jdeiglma@ethz.ch

1. EXPERIMENTAL METHODS

Our work is based on identifying and modelling all couplings that are relevant for the interactions of Rydberg atoms with their environment. Starting from a precise determination of the properties of isolated cesium Rydberg atoms, such as quantum defects [4] and hyperfine coupling constants [5], we have in recent years explored experimentally the interaction between cesium Rydberg and ground-state atoms [6–8], the millimeter-wave spectra and ionization dynamics of dipole-dipole-coupled Rydberg atoms [9], the role of terms beyond the dipole-dipole coupling in long-range Rydberg-atom pairs [10], and the properties of cesium Rydberg macrodimers [2].

Exemplary potential-energy curves of the investigated dimers are depicted in the left panel of Fig. 1. Here, and in the following, we call a "long-range Rydberg molecule" a molecule in which a single electron was excited to a high-n Rydberg state. Dimers, which are bound purely by the van der Waals forces between two atoms in Rydberg states, are called "macrodimers". The typical binding energy of both types of molecules is about 0.1 J/mol and is orders of magnitude smaller than the kinetic energy of the particles at room temperature (about 2 kJ/mol) and their electronic excitation energy of up to 700 kJ/mol. We therefore use very cold gases as a starting point for our investigations, which have kinetic temperatures around 40 µK, *i.e.*, kinetic energies of less than 1 mJ/mol. Gases with such low kinetic temperatures can only be prepared by the techniques of laser cooling, which are most easily implemented for alkali atoms. We use cesium, but the results can be qualitatively transferred to isoelectronic systems, because the structure of the investigated molecules results from the universal character of Rydberg atoms.

Direct transitions into the above described molecular Rydberg states from a covalently bound ground-state dimer are forbidden by the Franck-Condon principle, because initial and final states have extremely different binding lengths, as illustrated in the left panel of Fig. 1. Special experimental methods are therefore needed, and we employ photoassociation spectroscopy as depicted in Fig. 1 [11, 12]. The experiment proceeds as follows: The source of cesium atoms is a piece of high-purity cesium metal, placed in a flange attached to an ultra-high-vacuum chamber. Already at room temperature, the vapor pressure of cesium is rather high (around 10^{-6} mbar) and heating of the flange is not necessary. The cesium vapor diffuses through a valve into the main chamber where we operate a magneto-optical trap (MOT), a device developed in atomic physics [13].

In a MOT, laser beams red-detuned from a strong cycling transition exert slowing forces on the atoms, which eventually accumulate at the zero point of a three-dimensional magnetic-field gradient. Within a few seconds, we typically trap 10^7 cesium atoms at a density of 10^{11} cm^{-3} and a temperature of 40 µK. We can increase the density to about 10^{12} cm^{-3} by transferring the atoms into an optical dipole trap, an optical-tweezer-like device that traps the atoms at the intensity maximum of an intense red-detuned laser beam.

To associate these ultracold cesium atoms into molecules, a continuous-wave (cw) UV laser beam, the frequency of which has been shifted to the red from a transition into an atomic $n^2\mathrm{P}_j$ state, illuminates the atomic cloud. A pair of freely scattering atoms in the dissociation continuum of the two lowest electronic states of the Cs_2 dimer ($\mathrm{X}^1\Sigma_g^+$ and $\mathrm{a}^3\Sigma_u^+$) may now absorb a photon and form a bound, long-range Rydberg molecule if the following two conditions are fulfilled: *i)* the interatomic separation matches the bond length, and *ii)* the detuning of the laser matches the binding energy of a rovibronic dimer state. To detect the successful formation of a dimer, we apply high-voltage pulses with field amplitudes up to 1 kV/cm, which ionize the Rydberg molecules. The resulting ions are then detected on a microchannel-plate detector [5] (see Figure 1). Autoionization of Rydberg molecules is detected by applying weak electric-field pulses, which have sufficient amplitude to extract the resulting ions but which are too weak to field ionize neutral Rydberg molecules. We acquire an excitation spectrum by varying the detuning of the laser frequency while simultaneously recording the detected ion yield.

Photoassociation spectroscopy of the doubly-excited macrodimers is somewhat more complicated, because simultaneous absorption of two photons by a pair of ground-state atoms requires rather high intensities which cannot be achieved using narrowband cw lasers. Such intense laser pulses can also cause unwanted light-induced energy shifts (AC Stark shifts). Our early studies using a pulse-amplified dye laser system with a transform-limited resolution of 140 MHz yielded important insights into non-adiabatic couplings in Rydberg-atom pairs and were instrumental in developing an accurate theoretical model for their interactions [10, 14] but lacked the spectral resolution to unambiguously identify the spectral signatures of macrodimers. We thus implemented a sequential photoassociation scheme: a first pulse excites a few ground-state atoms into a $n^2\mathrm{P}_j$ (one-photon excitation) or a $n^2\mathrm{S}_{1/2}$ (two-photon excitation) Rydberg state. The actual photoassociation occurs when an excited Rydberg atom and a ground-state atom are found at the right distance and absorb a second photon from a narrowband cw UV laser, the frequency of which is detuned from a transition to a $n^2\mathrm{P}_j$ state [2]. This sequential scheme allows us to perform the spectroscopy of macrodimers with a resolution limited by the cw laser. In the following, we will first discuss the singly-excited long-range Rydberg molecules, and then focus in more detail on our investigations on doubly-excited macrodimers.

2. LONG-RANGE RYDBERG MOLECULES

The mean interparticle separation in a gas at room temperature and atmospheric pressure is about 2 nm. If one excites alkali atoms to Rydberg states in such a gas, a large number of ground-state particles will be within the orbit of the Rydberg electrons. Surprisingly, even under such conditions, reasonably sharp Rydberg lines can be observed, which are, however, shifted in energy. The magnitude of this shift is directly proportional to the pressure of the background gas, while the sign of the shift depends on the chemical nature of the gas. This effect was already noted in the 1930s by Amaldi and Segrè in Rome [15], and for lower valence states by Füchtbauer and coworkers in Rostock [16]. Simple perturbation arguments, which treat the background gas as a dielectric medium, predict indeed a shift, which increases linearly with pressure, but only towards lower transition energies. Enrico Fermi realized that an additional contribution needs to be considered, namely the scattering of the Rydberg electron off the perturbers [17]. He approximated the effect of the long-range scattering potential by a contact-type pseudopotential, parametrized by a single parameter, the scattering length. Both concepts, the pseudopotential and the scattering length, were first introduced in this context and later found most important applications in nuclear physics. For the resulting shift, Fermi derived the following simple expression (in atomic units)

$$\Delta E = 2\,\pi\,a\,\rho, \tag{1}$$

where a is the scattering length and ρ is the number density of the perturbers. The value of the scattering length depends on the chemical nature of the perturbers and can be positive or negative.

Following the same derivation, one obtains the expression for the interaction of the Rydberg electron with a single perturber,

$$V = 2\,\pi\,a\,|\Psi(R)|^2, \tag{2}$$

where $|\Psi(R)|^2$ is the modulus squared of the Rydberg-electron wave function at the position of the perturber. Equation (2) predicts an oscillatory interaction potential between a Rydberg atom and a ground-state atom,

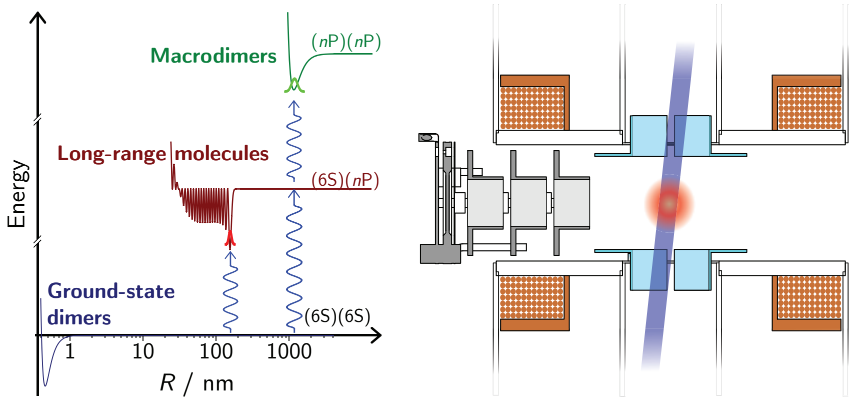

Fig. 1: (left) Photoassociation scheme: Two freely scattering atoms absorb one or two UV photons and form a bound dimer in an electronically excited state. (Right) Experimental setup: Ultra-high-vacuum chamber (indicated by thin lines) with magnetic coils for laser cooling (brown), electric-field plates for the application of compensation and ionization fields (light blue), cloud of laser-cooled atoms (red), UV excitation laser (blue) and ion detector (gray).

with a large number of potential minima supporting bound vibrational states. Detailed quantum-chemical calculations confirmed this prediction for lower valence states [18], but are not feasible for highly-excited Rydberg states. In the derivation of Eq. (1) Fermi assumed that only s-wave scattering contributes to the interaction. This is justified close to the classical outer-turning point of the Rydberg orbit, where the semiclassical kinetic energy of the Rydberg electron becomes very small. The theory was extended to higher collision energies by Omont [19] and was applied very successfully to calculations of the energy structure of alkali-rare-gas dimers [20].

The mean interparticle separation in ultracold gases is on the order of 1 µm, corresponding to densities of about $10^{12}\,\mathrm{cm}^{-3}$. Thus, there is at most one perturber atom within the Rydberg electron's orbit, whose diameter can be approximated, for low angular momentum states, by $2n^2a_o$ (*i.e.*, 100 nm at $n \sim 30$). Under these conditions, photoassociation can be used to form dimers in the oscillatory potentials predicted by Eq. (2) [3, 21]. The depth of the potential minima is inversely proportional to the effective volume enclosed by the Rydberg-electrons orbit, and hence scales with n as n^{-6}. As in covalently-bound alkali dimers, the spins of the valence electrons can either couple in singlet or triplet configuration, resulting in very different covalent-bond strengths. The dimer $\mathrm{X}^1\Sigma_\mathrm{g}^+$ ground state of Cs_2 has, for example, a dissociation energy of about $5800\,\mathrm{cm}^{-1}$, while the lowest triplet state $\mathrm{a}^3\Sigma_\mathrm{u}^+$ is bound by only $290\,\mathrm{cm}^{-1}$ [22]. In the case of long-range Rydberg alkali dimers, the spin configuration influences the binding energies very differently, and only indirectly, via the spin-dependent electron-Cs scattering lengths. The triplet scattering length is rather large and negative, while the singlet scattering length is much smaller and for the lighter species even positive. It was thus expected that only triplet scattering contributes to the binding, and that singlet scattering can be neglected [3]. A model including only triplet scattering indeed successfully reproduced the first observations of long-range Rydberg molecules [21, 23]. Only recently it was noted that the large hyperfine interaction in the ground-state atom mixes triplet and singlet scattering channels and that both contributions need to be considered [6, 24, 25].

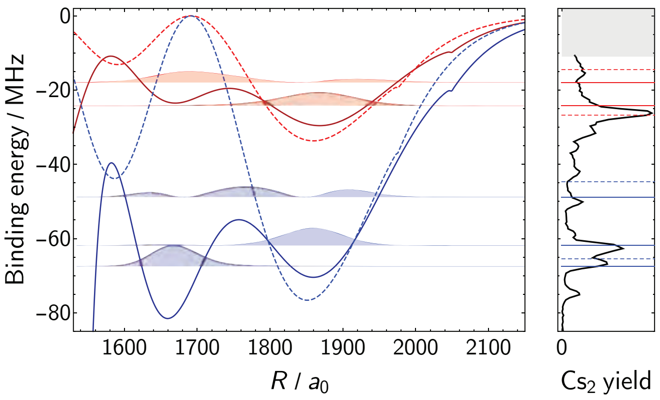

Fig. 2: (Left) Calculated potential energy curves including s- and p-wave contributions for $[6^2\mathrm{S}_{1/2}\,(F' = 4)\,35^2\mathrm{P}_{3/2}]$ long-range Rydberg molecules with pure triplet character $^3\Sigma_\mathrm{g}^+$ (thick blue) and mixed singlet-triplet character $^{1,3}\Sigma_\mathrm{g}^+$ (thick red). The quantum number F' indicates the hyperfine quantum number of the ground state atom, which remains an approximate quantum number in the dimer. Thin lines sketch the few lowest vibrational wave functions in each potential. For comparison, the potential energy curves calculated in Ref. [6] in the s-wave-scattering approximation are shown as dashed lines. On the right, an experimental spectrum (black line) is compared to calculated binding energies in the s- plus p-wave (solid) and only s-wave (dashed) approximations.

Typical potential energy curves of Cs $n^2\mathrm{P}_J$ long-range Rydberg molecules are depicted in Fig. 2 for n = 35, where the oscillatory nature of the potential energy curves becomes clearly visible. In the figure, calculations including only s-wave scattering (dashed lines) are compared to calculations including s- and p-wave scattering (solid lines). Large deviations become visible when the semiclassical energy of the Rydberg electron approaches the energy of a p-wave shape resonance in the electron-Cs scattering (here at an internuclear distance of about 1500 a_0). At this resonance, the Rydberg electron becomes briefly trapped behind the rotational barrier of the rotating Cs^- scattering complex, significantly enhancing the elastic scattering rate. The binding energies of the lowest vibrational states in the outermost minima, however, can reproduce the positions of the strongest experimental resonances in both calculations rather well. Only the p-wave calculation seems to reproduce the observed splitting of the resonance at −65 MHz.

In Fig. 3, experimental photoassociation spectra recorded in the vicinity of $n^2\mathrm{P}_{3/2}$ Rydberg states (n = 26, ..., 34) are shown. In all measurements, strong molecular resonances are observed at energies which are expected from a s-wave scattering model including only triplet scattering (indicated by vertical blue lines). Strong additional resonances (marked in red and green) are also observed, the energies of which depend on the initial hyperfine state of the ground-state atoms before photoassociation. In Ref. [6], we could attribute these additional resonances to previously unobserved electronic states resulting from a combination of triplet and singlet scattering channels. A full model, including the energy dependence of the s-wave scattering length, singlet and triplet scattering channels, and the hyperfine interaction of the ground-state atom, reproduced the binding energies of all 36 assigned resonances after only two parameters (the zero-energy singlet and triplet s-wave scattering lengths) were adjusted (see right panel of Fig. 3). Even the deviation from the expected n^{-6} scaling for the $[6^2\mathrm{S}_{1/2}(F' = 3)32^2\mathrm{P}_{3/2}]\ {}^{1,3}\Sigma_\mathrm{g}^+$ state is reproduced by the model and can be attributed to an accidental degeneracy of the ground-state hyperfine splitting and the spin-orbit splitting of the Rydberg atom at this value of n.

The values of the zero-energy s-wave scattering lengths, determined by matching experimental and calculated resonance positions in Ref. [6] and shown in Table I, represent their first experimental determinations. A full *ab-initio* calculation of these quantities is beyond the capabilities of current theories. However, modified effective-range theory can extrapolate measurements at higher collisions energies to the zero-energy limit [26]. A comparison with our experimental values (see Table I) shows very good agreement for the triplet scattering channel, while the values for singlet scattering deviate. We are currently exploring the model-dependence of the extracted scattering lengths, especially the influence of the various approximations made in the calculations [27, 28]. Our goal is to extend these experimental and theoretical studies to a wider range of systems. We have recently extended our setup to allow for the investigation of heteronuclear dimers, and envision an extension to larger molecules, for which laser cooling could be demonstrated recently [29, 30].

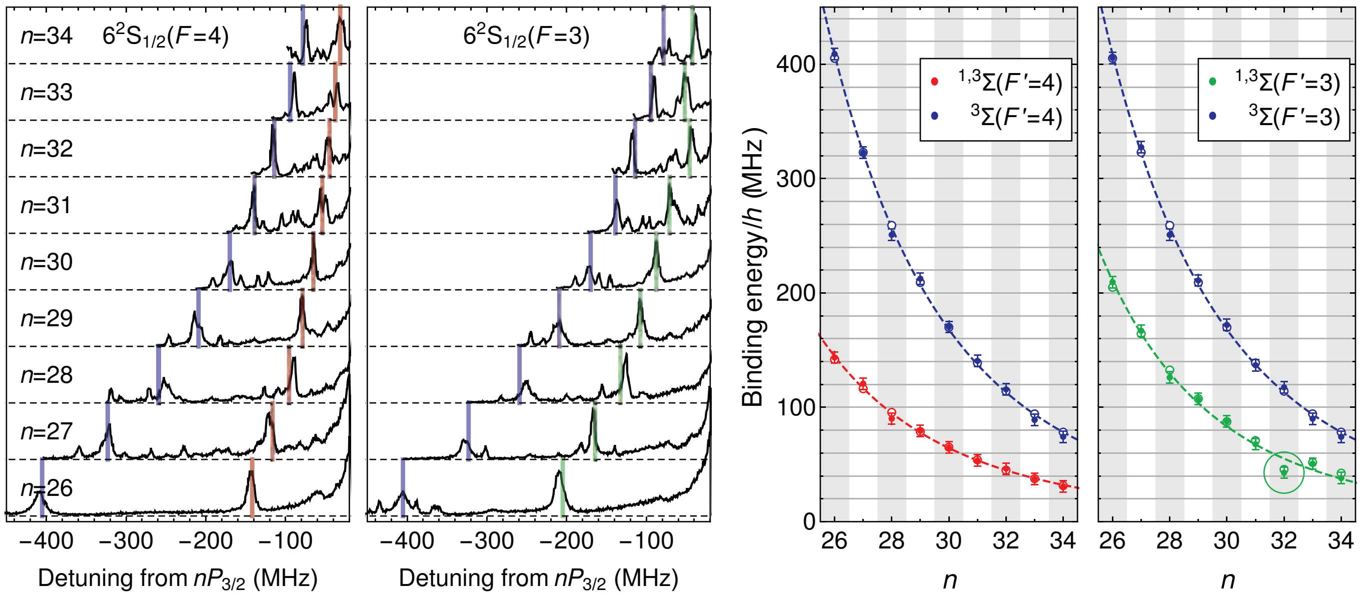

Fig. 3: (Left) Experimental photoassociation spectra recorded for red detunings from $n^2P_{3/2}$ Rydberg states after preparing all atoms in either the $F = 3$ or $F = 4$ component of the $6^2S_{1/2}$ ground state. The atomic transition at zero detuning is strongly saturated and thus not shown. The calculated binding energies of the vibrational ground states of the $^3\Sigma_g^+$ (blue) and the $^{1,3}\Sigma_g^+$ (red/green) states are indicated by vertical opaque lines. (Right) Comparison of all measured $\nu = 0$ binding energies (symbols with error bars) with the calculated line positions (open circles). The qualitative scaling of $E_{\nu=0}(n) \propto n^{-6}$ is indicated by dashed lines. The deviation from this scaling for $[6^2S_{1/2}\,(F' = 3)\ 32^2P_{3/2}]\ ^{1,3}\Sigma_g^+$ is highlighted by a green circle and discussed in the text.

Channel	Exp [6]	Theory [26]
^{3}S	-21.8(1) a_0	-21.7 a_0
^{1}S	-3.5(2) a_0	-1.33 a_0

Table I. Comparison of the experimental values of zero-energy triplet and singlet scattering lengths (in Bohr radii a_0) [6] with theoretical values, which were obtained by extrapolation from higher-energy scattering data using a relativistic modified effective range theory [26].

3. INTERACTIONS OF TWO RYDBERG ATOMS

In the following, we will consider the interactions when both atoms are in a Rydberg state. An atom in a Rydberg state has an internal energy close to the ionization energy of the atom (typically a few electron volts). In an encounter of two Rydberg atoms, there is thus sufficient energy to ionize one of the atoms even at vanishing kinetic energies, and one might expect rapid autoionization of the complex. We have indeed observed such a Penning-type autoionization of Rydberg-atom pairs at short interatomic distances in previous experiments [9]. However, the ionization rates become only appreciable at distances where the electronic orbitals of the two Rydberg-electrons overlap [31, 32]. Towards larger distances, where the van der Waals interactions between Rydberg atoms are still strong but covalent interactions become negligible, ionization rates are strongly suppressed and much smaller than the radiative decay rates of the Rydberg atoms [33]. The reason for this suppression is that at large distances, the atoms can exchange energy only by emission and absorption of photons, and threshold-photoionization rates of Rydberg atoms are very small.

A useful criterion for the separation of the two regions of covalent electronic interaction at short internuclear distances and pure long-range van der Waals interactions at large distances, is the Le Roy radius [34]

$$R_{LR} = 2\left(\sqrt{r_A^2} + \sqrt{r_B^2}\right), \tag{3}$$

where $r_i^2 = \langle\phi_i|r^2|\phi_i\rangle$ quantifies the extent of the electronic wavefunction ϕ_i of atom i. For interatomic distances larger than R_{LR}, electron-exchange integrals are negligible. The interaction energy between the two Rydberg atoms A and B at a distance R is then conveniently expressed in the multipole expansion [35, 36]

$$V(R) = \sum_{L_{A,B}=0}^{\infty} \sum_{\omega=-\min L_A,L_B}^{\min L_A,L_B} \frac{(-1)^{L_B} f_{L_A L_B \omega}}{R^{L_A+L_B+1}} \Omega_{L_A\omega}\Omega_{L_B-\omega} \tag{4}$$

where explicit expressions for the components ω of the multipole moments $\Omega_{L\omega}$ with order L, and the angular factors $f_{L_A L_B \omega}$ can be found, *e.g.*, in Ref. [14]. The interaction operator $V(R)$ converges asymptotically to the exact coulombic interaction energy [37]. It lends itself to be evaluated in a basis of product states of atomic wavefunctions centered at atom A and atom B, $|\phi_A\rangle|\phi_B\rangle$, in which the multipole moments of the Rydberg atoms can be calculated analytically with high precision. The only input parameters to such a calculation are experimentally determined quantum defects, angular-dependent model potentials for the electron-core interaction, and the choice of the atomic basis sets.

3.1 SCALING OF RYDBERG-RYDBERG INTERACTIONS

Because Rydberg atoms are neutral, their zeroth-order multipole moments Ω_{00} vanish. The first non-vanishing permanent multipole moments are the quadrupole moments of states with angular momentum $l \geq 1$. One actually finds that the largest contributions to the total interaction energy between two

Rydberg atoms do not stem from permanent multipole moments, but from transition moments. This fits very well London's idea that charge fluctuations in one atom induce charge fluctuations in the other atom [38]. The first non-vanishing term of the multipole expansion between two neutral atoms is the dipole-dipole interaction with $L_\mathrm{A} = L_\mathrm{B} = 1$, scaling with R as R^{-3}. The binding energy of the electron in a Rydberg state n is given by the Rydberg-Ritz formula $E_{nl} = -\dfrac{h\,c\,R_{Cs}}{(n-\delta_l)^2}$, where h is Planck's constant, c the speed of light, R_Cs the Rydberg constant for cesium, and δ_l the series-dependent quantum defect. The strongest coupling is found between states with comparable effective principal quantum number $\tilde{n} = n - \delta_l$, for which the transition dipole moments (in atomic units) can be approximated by $\frac{3}{2}\tilde{n}^2$ [39]. The strength of a resonant dipole-dipole interaction, such as the coupling between a $|n\,s\rangle|n\,p\rangle$ and a $|n\,p\rangle|n\,s\rangle$ state, then scales as n^4 (see equation (4)).

The interaction between two atoms in the same initial state $|n\,l\rangle|n\,l\rangle$ is dominated by off-resonant couplings to nearly degenerate pair states $|n'\,l'\rangle|n''\,l''\rangle$. For the case $\tilde{n} \sim \tilde{n}' \sim \tilde{n}''$, the energy defect of the coupled states

$$\Delta E = 2E_{nl} - E_{n'l'} - E_{n''l''} \qquad (5)$$

scales as $\tilde{n}^{-3}$ and the coupling matrix element $V_\text{dip–dip}$ as $\tilde{n}^4$. Second-order perturbation theory yields an energy shift [39, 40]

$$E_\text{dip-dip} = \left(\frac{V_\text{dip-dip}}{R^3}\right)^3 \frac{1}{\Delta E} \propto \frac{n^{11}}{R^6}. \qquad (6)$$

The exceptional scaling of $E_\text{dip-dip}$ with the eleventh power of n was found to be valid over a large range of Rydberg states [41], but is sometimes broken, *e.g.*, when the energy defect (Eq. (5)) becomes very small or changes sign. The R^{-6} scaling of the off-resonant dipole-dipole interaction is the well-known leading order of the van der Waals interaction between two neutral atoms without resonant interactions. Such a simple perturbative treatment of the interaction between two Rydberg atoms of course only yields qualitative results. First, the angular dependence of the interaction operator V was neglected, and second, the treatment by second-order perturbation theory is not valid anymore at distances where significant state mixing occurs. In the next section, we will introduce a different approach, which yields potential energy curves and molecular transition dipole moments with spectroscopic accuracy.

In passing, we note that for very large internuclear separations one would have to consider the effects of retardation of the Coulomb interaction due to the finite speed of light [42]. An estimate for the distance, beyond which the description of the interaction by Eq. (4) fails, is given by

$$R_\text{ret} = \frac{\lambda_\text{max}}{2\pi} = \frac{hc}{2\pi \max\,(E_{n_i l_i} - E_{n_f l_f})}, \qquad (7)$$

where λ_max is the wavelength corresponding to the largest energy difference between interacting states. Because the strongest couplings occur between states with $\Delta\tilde{n} \leq 1$, the value of this energy difference can be estimated from $2(E_{n_i l_i} - E_{n_f l_f}) \approx 4\,\frac{R_{Cs}}{\tilde{n}^3}$, which yields

$$R_\text{ret} = \frac{\tilde{n}^3}{8\pi R_{Cs}}. \qquad (8)$$

For a pair of Rydberg atoms in a state with $\tilde{n} \sim 20$ one finds a distance of around 30 µm beyond which retardation effects need to be considered. This distance, which increases with $\tilde{n}$ as $\tilde{n}^3$, is much larger than the internuclear separations encountered in our work up to now.

3.2 CALCULATION OF INTERACTION POTENTIALS

The total Hamiltonian of two interacting Rydberg atoms in the nonrotating frame is given by

$$H = H_0^\mathrm{A} + H_0^\mathrm{B} + V, \qquad (9)$$

where $H_0^\mathrm{A,B}$ are the Hamiltonians of the isolated atoms including the atomic spin-orbit interaction. Spin-spin and spin-other-orbit interactions can be neglected in the van der Waals region. The hyperfine coupling in high-n Rydberg atoms can in general also be neglected when considering Rydberg-atom pair states, because atomic hyperfine splittings are typically not resolved in the optical excitation of high-n Rydberg states [5]. In order to obtain the adiabatic potential-energy curves of a Rydberg-atom pair, H is numerically evaluated in matrix form using the product basis $|n_A l_A j_A \omega_A\rangle|n_B l_B j_B \omega_B\rangle$. The quantum numbers $j_{A,B}$ and $\omega_{A,B}$ indicate the electronic angular momentum including spin of the two Rydberg atoms and their projection on the internuclear axis, respectively. Because $\Omega = \omega_A + \omega_A$ is conserved under the Hamiltonian H, we set up the matrix representation of H separately for each value of Ω. It would be computationally advantageous to express the Hamiltonian in a basis of symmetrized wavefunctions, however our approach allows for the straightforward inclusion of non-adiabatic couplings in the rotating molecule [10].

Because Equation (4) expresses the interaction operator as an infinite sum of multipole terms, for numerical evaluation this sum needs to be truncated at some point. A restriction to terms up to the octupole-octupole interaction ($L_{A,B} = 3$) term was sufficient for the calculation to converge to the experimental resolution, but this limit depends strongly on the investigated molecular feature [14]. Multipole moments are derived by numerical integration of radial integrals on the basis of experimental quantum defects and a l-dependent model potential, while the angular integrals are calculated analytically. The pair-state energies and wavefunctions are then found as a function of internuclear separation by determining eigenvalues and eigenvectors of the matrix-representation of H.

This computational approach only yields an accurate representation of the true energy spectrum of the Hamiltonian (9) if the basis states allow for an accurate representation of the electronic structure. Because the number of excited pair-state asymptotes is extremely large (and in principle infinite), in practice the basis states can only represent the electronic structure in a certain energy interval around one pair-state asymptote of interest. In Ref. [14] we have defined a useful set of criteria and outlined methods to test the convergence of the computational approach. The importance of carefully investigating the influence of the chosen basis set is illustrated in Fig. 4. The left panel depicts the result of a calculation for the central pair-state asymptote $69^2\mathrm{S}_{1/2}72^2\mathrm{S}_{1/2}$ in rubidium, reproducing results of Ref. [43] using a similar set of basis states. According to Eq. (3), the Le Roy radius for this pair state is 1.5 µm. At larger distances, the Rydberg-Rydberg interactions are accurately described by the Hamiltonian (9). The potential-energy curves with clearly visible minima at $R \sim 2.1$ µm and $D_0 \sim 1.0$ GHz were predicted in Ref. [43] to support bound vibrational states, the so-called "macrodimer" states. The calculation shown on the right-hand side of Fig. 4 was performed for the same central pair-state asymptote, but with an increased basis set constructed according to our criteria. The dimension of the basis set is increased from about 80 states to almost 3000 to reach convergence with respect to the structure of the potential-energy curves around the predicted minima. Because the density of electronic states becomes too large for a complete graphical presentation, the results of the calculation are presented in an optimized way: all electronic states are drawn as thin gray lines. Only states with significant (*i.e.*, more than 3 %) character of the asymptotic $69^2S_{1/2}72^2S_{1/2}$ state are highlighted by black and red lines for $\Omega = 0$ and $\Omega = 1$, respectively. Additionally, the intensity of the color is proportional to the amount of $69^2S_{1/2}72^2S_{1/2}$ character a state has at a certain distance. While the two calculations agree qualitatively for internuclear separations larger than 4 µm, significant deviations become apparent for smaller values of R. The inclusion of basis states with high angular momentum ($l \geq 4$) reveals that the region of minima in the potential-energy curves discussed above is strongly perturbed, and that the asymptotic electronic character diffuses over many closely spaced electronic states. This indicates a breakdown of the Born-Oppenheimer approximation, and makes it very unlikely that vibrationally-bound dimers can exist close to this central pair-state asymptote.

3.3 SIMULATION OF SPECTRAL FEATURES AND COMPARISON TO EXPERIMENTS

Potential-energy curves such as the one shown in Fig. 4 cannot be measured directly. However, they lead to complex, asymmetric line broadenings and to the appearance of satellite peaks when Rydberg states are excited in dense, cold gases [9, 10, 44–47]. The most direct comparison between experimental observations and theory can be made by simulating the experimental spectra on the basis of the calculations presented in the previous section. In the following, we concentrate on an experimental setting where the Rydberg-atom-pair states are excited by the simultaneous absorption of two photons from a single, intense laser beam [9, 10, 45].

To model the excitation spectrum of two ground-state atoms into Rydberg-atom-pair states we assume that *i)* the relative motion of the atoms can be treated classically, *ii)* the spatial density distribution of ground-state atoms is homogeneous, *iii)* the angle between the internuclear axis and a laboratory-fixed axis is randomly distributed, and *iv)* the excitation probability per ground-state-atom pair is much smaller than one. Assumption *i* is justified in our experiments because the excitation occurs at distances much larger than the thermal de Broglie wavelength of the atoms ($\lambda_{\text{th}} \sim 30$ nm at $T = 40$ µK). The probability of exciting a pair of ground-state atoms into a Rydberg-atom-pair state at an internuclear separation R is then proportional to the probability of finding the pair of atoms at distance R. In a homogeneous medium (assumption *ii*), the number of pairs with distance R is proportional to R^2. In the case of low excitation probabilities (assumption *iv*), the excitation probability is then also proportional to R^2.

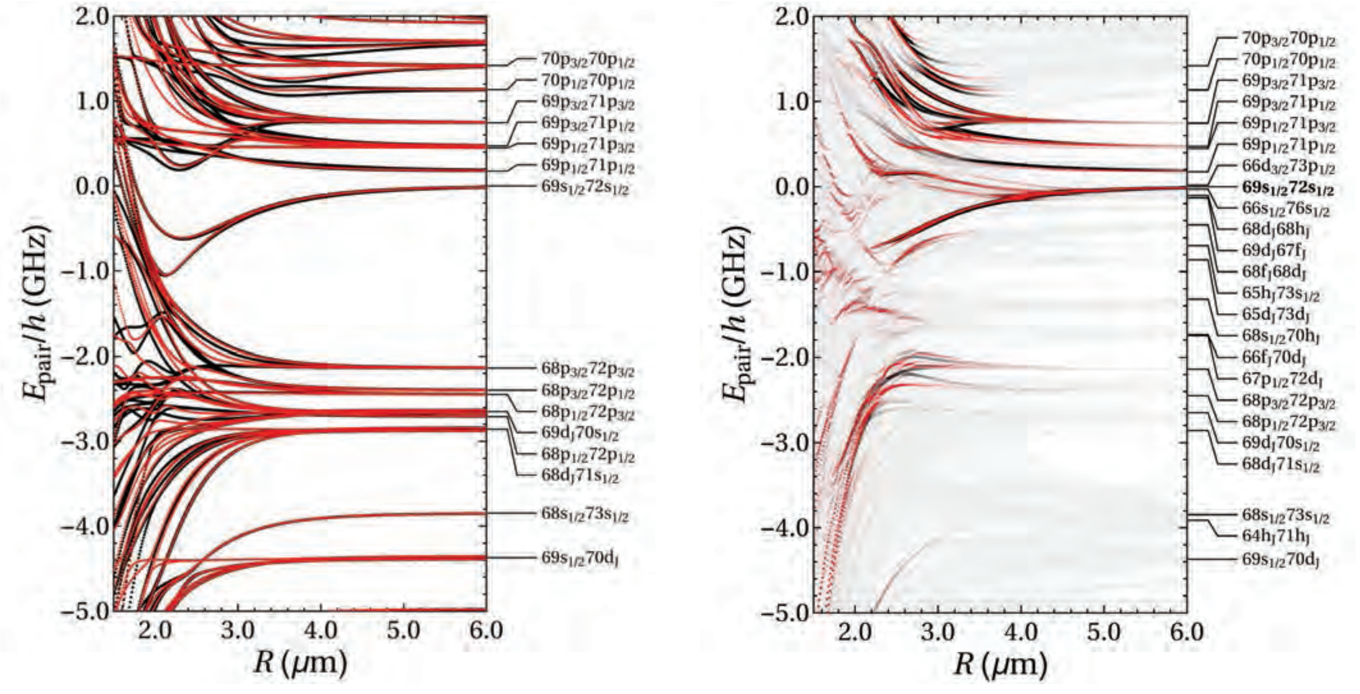

Fig. 4: Calculated potential-energy curves for a rubidium Rydberg-atom pair close to the $69^2S_{1/2}72^2S_{1/2}$ asymptote using different basis sets: (Left panel) basis set chosen as in Ref. [43], (right panel) converged basis set. Black and red curves correspond to states with $\Omega = 0$ and $\Omega = 1$, respectively. In the right panel, the intensity of the color codifies the $69^2S_{1/2}72^2S_{1/2}$-character of the state, as discussed in the text (gray: 0%, full color: >3%). The energies of selected basis states are indicated on the right hand side of each figure (the label h indicates "hydrogenic" states with $l \geq 4$, for which the quantum defect δ_h is zero). All energies are given with respect to the asymptotic energy of the $69^2S_{1/2}72^2S_{1/2}$ pair state.

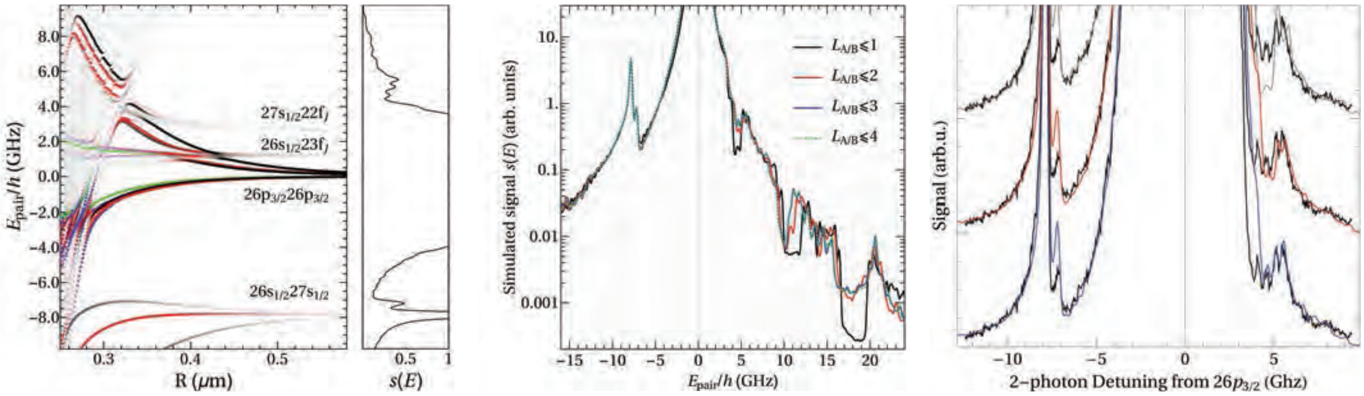

Fig. 5: (Left) Potential-energy functions and simulated spectrum near the cesium $26^2P_{3/2}26^2P_{3/2}$ pair-dissociation asymptote with multipole terms $L_i \leq 3$ included in the calculation. Black, red, blue, and green curves correspond to states with $\Omega = 0, 1, 2$, and 3, respectively. The intensity of the color codifies the TDM of the electronic states (gray: 0%, full color: > 1% of the atomic $26^2P_{3/2}\leftarrow 6^2S_{1/2}$ TDM). (Middle) Simulated spectra $s(E)$ (arb. units) based on calculations including only terms $L_i = 1$ (dipole-dipole), terms with $L_i \leq 2$ (up to quadrupole-quadrupole), terms with $L_i \leq 3$ (up to octupole-octupole), and terms with $L_i \leq 4$ (up to hexadecapole-hexadecapole). (Right) comparison of experimental two-photon spectrum around the Cs $26^2P_{3/2}$ Rydberg state (solid black line, shown three times) with the calculations shown in the middle panel. The different comparisons have been vertically offset for clarity: (top) $L_i = 1$, (middle) $L_i \leq 2$, (bottom) $L_i \leq 3$. All energies are given with respect to the asymptotic energy of the $26^2P_{3/2}26^2P_{3/2}$ pair state.

An example for asymmetric line broadening and more complex spectral satellite features encountered in the excitation of a dense gas of ground state atoms to Rydberg states is depicted in Fig. 5. Calculated potential energy curves around the cesium $26^2P_{3/2}26^2P_{3/2}$ pair-dissociation asymptote are shown together with the resulting simulated spectra. The calculated spectrum was folded with a Gaussian function with a full width at half maximum (FWHM) of 140 MHz. This corresponds to the typical resolution in experiments with pulse-amplified continuous-wave lasers [9, 10, 45]. The simulated spectrum in the left panel of Fig. 5 was rotated to highlight the correspondence between perturbations in the calculated potential-energy curves and features in the simulated spectrum, which are discussed in the following. Asymptotically, only the central pair state $26^2P_{3/2}26^2P_{3/2}$ can be excited. This corresponds to the strong signal at zero detuning, which is clipped in the shown spectra. As R decreases, the $26^2S_{1/2}27^2S_{1/2}$ pair state at an energy of −8.0 GHz acquires excitation probability due to strong dipole-dipole interactions with the $26^2P_{3/2}26^2P_{3/2}$ pair state. In the simulated spectrum, this leads to the appearance of a peak at the asymptotic energy of the $26^2S_{1/2}27^2S_{1/2}$ pair state with a red-degraded line-shape due to the overall interaction-induced shift of the pair state to lower energies. The upper $\Omega = 1$ component of this pair-state asymptote, however, first exhibits a shift towards higher energies as R decreases before eventually reaching a turning point and shifting towards lower energies. The presence of this maximum in the potential energy curve leads to the appearance of an additional resonance structure at around −7 Ghz in the simulated spectrum.

A much larger number of local potential-energy minima and maxima appear for pairs with energies higher than the central pair state. These extrema result from avoided crossings between curves correlated asymptotically to the $26^2P_{3/2}26^2P_{3/2}$ and $22^2F_J22^2F_J$ pair states, respectively, and lead to the appearance of complex structures in the simulated spectrum. The exact shape of these structures depends critically on the chosen truncation of the multipole expansion (Eq. (4)), as demonstrated by the simulated spectra shown in the middle panel of Fig. 5. These spectra were derived from calculations of potential-energy curves where the multipole expansion was truncated after the dipole-dipole ($L_{A,B} = 1$), the quadrupole-quadrupole ($L_{A,B} \leq 2$), the octupole-octupole ($L_{A,B} \leq 3$), or the hexadecapole-hexadecapole ($L_{A,B} \leq 4$) term, respectively. While the spectrum around the $26^2S_{1/2}27^2S_{1/2}$ pair-state asymptote is already fully converged for ($L_{A,B} = 1$) within the chosen experimental resolution, the convergence of the calculated spectrum at higher energies requires the inclusion of terms up to the octupole-octupole term. This demonstrates that the convergence of all calculations has to be verified with respect to the chosen pair-state basis and the truncation of the multipole-expansion.

The right panel of Fig. 5 compares these calculations to an experimental spectrum, which was recorded using intense pulses from a pulse-amplified cw dye laser. This comparison, which was performed for a range of Rybderg-pair-state asymptotes ($n = 22$ to 26) in Ref. [9], demonstrates that the inclusion of octopole-octopole terms is indeed required to reproduce the complex resonance structures at positive detunings. The drawn experimental signal is proportional to the number of autoionizing Rydberg-pair states, which exhibits a higher signal-to-noise ratio than the total Rydberg-excitation signal, especially for the resonances at positive detunings. The overestimation of the strength of the pure dipole-dipole-coupling features at negative detunings is attributed to a seemingly lower autoionization rate for these features. For detunings smaller than ~4 GHz, the density of off-resonantly excited Rydberg atoms reaches the threshold for fast many-body ionization and plasma formation [48]. These processes are not included in our model and the corresponding part of simulated and experimental spectrum is thus not shown.

3.4 FORMATION OF MACRODIMERS

The reliable and accurate calculation of Rydberg-Rydberg interaction potentials presented in the previous section was instrumental in finding the range of experimental parameters that allowed us to experimentally observe and study macrodimers. The left panel of Figure 6 displays the potential energy curves correlating asymptotically to a pair of Rydberg atoms in a $44^2P_{3/2}$ and a $45^2S_{1/2}$ state. These two states are coupled at large internuclear distances by resonant dipole-dipole interactions and the pair-state energies thus exhibit a R^{-3} scaling. Avoided crossings with states correlated to pairs of atoms with lower pair-state energy lead in some potential-energy curves to minima at intermediate distances. These curves are (by definition) macrodimer states. The vibrational frequencies of the states highlighted in Fig. 6 are about 1.5 MHz, comparable to our spectroscopic resolution [4]. Spontaneous decay and black-body-radiation-induced transitions limit the lifetime of dimers in these states to about 30 µs. Autoionization due to non-adiabatic couplings was estimated to occur on even longer timescales [14].

The right panel of Fig. 6 shows the clear spectral signatures of the photoassociation of macrodimers: a sharp peak at a detuning corresponding to photoassociation of dimers in the lowest vibrational levels, and a broad blue-detuned shoulder corresponding to the formation of macrodimers in vibrationally excited states. These signatures were first observed in Ref. [2] for the asymptotes $43^2P_{3/2}$-$44^2S_{1/2}$ and $44^2P_{3/2}$-$45^2S_{1/2}$. The agreement between independent theory and experiment allows for an unambiguous assignment of the experimentally observed features to the formation of macrodimers with bond lengths around 1.2 µm. The simulated spectrum was folded with a Gaussian with a FWHM of 5 MHz, significantly more than the experimental linewidth observed in the spectroscopy of isolated atomic features of about 1.5 MHz. The reason for this additional broadening is unclear, however it hints at the presence of interactions of the macrodimer with other Rydberg atoms. The lifetime of the Cs_2 macrodimers was found to be limited by autoionization into the $Cs+Cs^+$ continuum, with lifetimes on the order of 2 µs, much shorter than anticipated. Currently we attribute this reduction to interactions of the macrodimer with surrounding Rydberg atoms, *i.e.*, three-body interactions which break the symmetries protecting the macrodimer from approaching short internuclear distances where pairwise, Penning-type ionization is known to dominate. The observed broadening of the molecular resonances supports this interpretation. However, further experiments are necessary to study the density-dependence of the macrodimer-lifetimes to rule out any intrinsic, hitherto unidentified autoionization mechanism in the dimer.

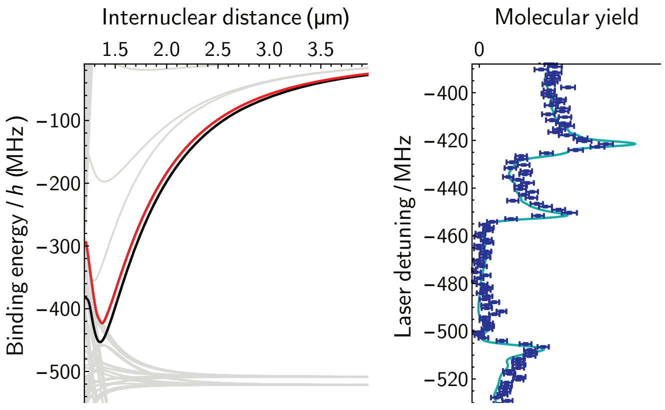

Fig. 6: (Left) Interaction potentials (gray) between a $44^2P_{3/2}$ and a $45^2S_{1/2}$ Rydberg atom. Selected macrodimer states with symmetry 0_u (black) and 1_g (red) are highlighted. (Right) Experimental molecular signal (blue points with errorbars) as function of the cw laser detuning from the $44^2P_{3/2}$ state and *ab-initio* simulation of the photoassociation rate (light-blue curve). The peaks at -450 and -420 MHz detuning correspond to the formation of macrodimers in the states highlighted in the left panel. The peak at -510 MHz correspond to the excitation of Rydberg-atom pairs on repulsive interaction potentials.

Theory predicts also the existence of stable configurations of three Rydberg atoms, so called "macrotrimers" [49]. The spectroscopy of such trimers, and larger oligomers, using photoassociation is even more challenging than the one of the macrodimers presented here, because of the even larger number of possible non-adiabatic couplings to dissociative and ionizing channels. A very promising perspective in this context is the study of Rydberg interactions between atoms that have been precisely positioned using optical tweezers [50]. The development of these experimental techniques opens the way to fully control nuclear and electronic motions in photoassociation spectroscopy.

ACKNOWLEDGMENTS

This article is based on extracts from previous reviews of the *long-Range interactions between Rydberg atoms* (J. Deiglmayr, Physica Scripta 2016, **91**, 104007), and *electronically highly excited molecules* (M. Peper and J. Deiglmayr, to appear in *Nachrichten aus der Chemie*). This work was supported financially by the ETH Research Grant ETH-22 15-1, the Swiss National Science Foundation under Project Nr. 200020-159848, and the NCCR QSIT of the Swiss National Science Foundation. I thank first and foremost Prof. Frédéric Merkt (ETH Zurich) for his continuous and exceptionally strong support. I also thank my coworkers Dr. Heiner Saßmannshausen, Michael Peper, Holger Herburger, Jonas Butscher, and Felix Helmrich for the very fruitful collaborations leading to the results presented in this article.

REFERENCES

[1] C. Boisseau, I. Simbotin, and R. Côté, *Phys. Rev. Lett.* **88**, 133004 (2002).

[2] H. Saßmannshausen and J. Deiglmayr, *Phys. Rev. Lett.* **117**, 083401 (2016).

[3] C. H. Greene, A. S. Dickinson, and H. R. Sadeghpour, *Phys. Rev. Lett.* **85**, 2458 (2000).

[4] J. Deiglmayr, H. Herburger, H. Saßmannshausen, P. Jansen, H. Schmutz, and F. Merkt, *Phys. Rev. A* **93**, 013424 (2016).

[5] H. Saßmannshausen, F. Merkt, and J. Deiglmayr, *Phys. Rev. A* **87**, 032519 (2013).

[6] H. Saßmannshausen, F. Merkt, and J. Deiglmayr, *Phys. Rev. Lett.* **114**, 133201 (2015).

[7] H. Saßmannshausen, J. Deiglmayr, and F. Merkt, *CHIMIA Int. J. Chem.* **70**, 263 (2016).

[8] H. Saßmannshausen, J. Deiglmayr, and F. Merkt, *Eur. Phys. J. ST* **225**, 2891 (2016).

[9] H. Saßmannshausen, F. Merkt, and J. Deiglmayr, *Phys. Rev. A* **92**, 032505 (2015).

[10] J. Deiglmayr, H. Saßmannshausen, P. Pillet, and F. Merkt, *Phys. Rev. Lett.* **113**, 193001 (2014).

[11] K. M. Jones, E. Tiesinga, P. D. Lett, and P. S. Julienne, *Rev. Mod. Phys.* **78**, 483 (2006).

[12] J. Ulmanis, J. Deiglmayr, M. Repp, R. Wester, and M. Weidemüller, *Chem. Rev.* **112**, 4890 (2012).

[13] H. J. Metcalf and P. van der Straten, *Laser Cooling and Trapping* (Springer New York, 1999).

[14] J. Deiglmayr, *Phys. Scrip.* **91**, 104007 (2016).

[15] E. Amaldi and E. Segrè, *Il Nuovo Cimento* **11**, 145 (1934).

[16] C. Füchtbauer and F. Gössler, *Zeitschrift für Physik* **87**, 89 (1934).

[17] E. Fermi, *Il Nuovo Cimento* **11**, 157 (1934).

[18] A. Yiannopoulou, G.-H. Jeung, S. J. Park, H. S. Lee, and Y. S. Lee, *Phys. Rev. A* **59**, 1178 (1999).

[19] A. Omont, *Journal de Physique* **38**, 1343 (1977).

[20] F. Masnou-Seeuws, M. Philippe, and P. Valiron, Phys. *Rev. Lett.* **41**, 395 (1978).

[21] V. Bendkowsky, B. Butscher, J. Nipper, J. P. Shaffer, R. Löw, and T. Pfau, *Nature* **458**, 1005 (2009).

[22] P. Staanum, A. Pashov, H. Knöckel, and E. Tiemann, *Phys. Rev. A* **75**, 042513 (2007).

[23] J. Tallant, S. T. Rittenhouse, D. Booth, H. R. Sadeghpour, and J. P. Shaffer, *Phys. Rev. Lett.* **109**, 173202 (2012).

[24] D. A. Anderson, S. A. Miller, and G. Raithel, *Phys. Rev. A* **90**, 062518 (2014).

[25] T. Niederprüm, O. Thomas, T. Eichert, and H. Ott, *Phys. Rev. Lett.* **117**, 123002 (2016).

[26] C. Bahrim, U. Thumm, and I. I. Fabrikant, *J. Phys. B* **34**, L195 (2001).

[27] S. Markson, S. T. Rittenhouse, R. Schmidt, J. P. Shaffer, and H. R. Sadeghpour, *ChemPhysChem* **17**, 3683 (2016).

[28] M. T. Eiles and C. H. Greene, *Phys. Rev. A* **95**, 042515 (2017).

[29] E. S. Shuman, J. F. Barry, and D. DeMille, *Nature* **467**, 820 (2010).

[30] S. Truppe, H. J. Williams, M. Hambach, L. Caldwell, N. J. Fitch, E. A. Hinds, B. E. Sauer, and M. R. Tarbutt, *Nat. Phys.* **13**, 1173 (2017).

[31] F. Robicheaux, *J. Phys. B* **38**, S333 (2005).

[32] M. Kiffner, D. Ceresoli, W. Li, and D. Jaksch, *J. Phys. B* **49**, 204004 (2016).

[33] T. Amthor, J. Denskat, C. Giese, N. N. Bezuglov, A. Ekers, L. S. Cederbaum, and M. Weidemüller, *Eur. Phys. J. D* **53**, 329 (2009).

[34] R. J. Le Roy, in *Molecular Spectroscopy, Vol.* **1**, edited by R. F. Barrow, D. A. Long, and D. J. Millen (Royal Society of Chemistry, Cambridge, 1973) pp. 113–176.

[35] P. R. Fontana, *Phys. Rev.* **123**, 1865 (1961).

[36] M. R. Flannery, D. Vrinceanu, and V. N. Ostrovsky, *J. Phys. B* **38**, S279 (2005).

[37] L. Z. Stolarczyk and L. Piela, *Int. J. Quant. Chem.* **15**, 701 (1979).

[38] F. London, *Zeitschrift für Physik* **63**, 245 (1930).

[39] T. F. Gallagher and P. Pillet, in *Adv. At. Mol. Opt. Phys.*, Vol. **56**, edited by E. Arimondo (Academic Press, 2008) pp. 161–218.

[40] T. G. Walker and M. Saffman, *Phys. Rev. A* **77**, 032723 (2008).

[41] K. Singer, J. Stanojevic, M. Weidemüller, and R. Côté, *J. Phys. B* **38**, S295 (2005).

[42] H. Casimir and D. Polder, *Nature* **158**, 787 (1946).

[43] N. Samboy, J. Stanojevic, and R. Côté, *Phys. Rev. A* **83**, 050501 (2011).

[44] J. M. Raimond, G. Vitrant, and S. Haroche, *J. Phys. B* **14**, L655 (1981).

[45] S. M. Farooqi, D. Tong, S. Krishnan, J. Stanojevic, Y. P. Zhang, J. R. Ensher, A. S. Estrin, C. Boisseau, R. Côté, E. E. Eyler, and P. L. Gould, *Phys. Rev. Lett.* **91**, 183002 (2003).

[46] K. Afrousheh, P. Bohlouli-Zanjani, D. Vagale, A. Mugford, M. Fedorov, and J. D. D. Martin, *Phys. Rev. Lett.* **93**, 233001 (2004).

[47] K. R. Overstreet, A. Schwettmann, J. Tallant, and J. P. Shaffer, *Phys. Rev. A* **76**, 011403 (2007).

[48] T. C. Killian, T. Pattard, T. Pohl, and J. M. Rost, *Phys. Rep.* **449**, 77 (2007).

[49] N. Samboy and R. Côté, *Phys. Rev. A* **87**, 032512 (2013).

[50] C. Regal, *Science* **354**, 972 (2016).